RESEARCH ARTICLE   **OPEN ACCESS**

A PHILOSOPHICAL ANALYSIS OF AISI 316/AISI 410 STAINLESS STEEL JOINT BY MEANS OF MECHANICAL AND METALLURGICAL PROPERTIES USING TIG WELDING METHOD

Kathiresan G[1], Prabakaran M P[2], Govindarasan D[3] and Vairavel. M*[4]

[1] Professor, Excel Engineering College, Namakkal, Tamil Nadu, India.
[2] Associate Professor, Erode Sengunthar Engineering College - Erode, Tamil Nadu, India.
[3] Assistant Professor, AVS Engineering College - Salem, Tamil Nadu, India.
[4] Professor, Annapoorna Engineering College, Salem, Tamil Nadu, India.

[1] http://orcid.org/0000-0002-6428-4482, [2] http://orcid.org/0009-0001-5234-6156, [3] http://orcid.org/0009-0005-3062-728X
[4] http://orcid.org/0000-0002-8687-7887

Email: [1] kathirmechengg1980@gmail.com, [2] prabakaranmp89@gmail.com, [3] grajmech87@gmail.com, [4] phdannauniv2020@gmail.com

ARTICLE INFO	ABSTRACT
	This study employed Taguchi's Grey Relational Analysis (GRA) to assess the optimization of process boundaries. Improved metallurgical and mechanical qualities of Martensite (AISI 410) and Austenitic (AISI 316) stainless steel joints were the aim of the investigation. In order to do this, TIG welding experiments were carried out with different current flows, welding speeds, and shielding gas flow rates. Responses like tensile strength and microhardness were taken into consideration to determine the ideal procedure settings. Analysis of variance had been used to determine their impacts. The best set of parameters was found to be 10 lit/min shielding gas flow, 2 m/min welding speed, and 120-amp welding current based on the GRA. The distribution of alloys, the microhardness of different weld zones, and the characterisation of microstructural and mechanical properties were also investigated.

I. INTRODUCTION

Thermal power plants (TPPs) of today are made up of a lot of welded joints, either to meet design requirements or to save money. In those factories, a variety of welded joints were employed, such as those made of austenitic stainless steel (ASS) and martensic stainless steel (MSS) [1]. ASS and MSS materials can be welded with TIG, SMAW, SAW, LBM, and EBM, among other welding techniques [2], [3]. Nevertheless, TIG welding is the most widely used welding process for connecting tubes and pipes in TPP because of its superior productivity, consistency, minimal skill need, and virtue-sounding nature [4]. Austenitic and martensite stainless steels are utilised in super-heaters and re-heaters due to their resilience to deterioration, creep strength, and temperature stability [5].

MSSs, on the other hand, are a type of alloy composed of Fe and C-Cr, which has a BCT crystal structure. These materials are ferro-magnetic, hard, brittle, and heat-tolerant, making them a cost-effective option for water-evaporator and steam headers [6 - 8].

Ferritic stainless steel, nickel-based super-alloy, and creep strength increased austenitic/martensitic steel are the materials most frequently utilized in power plants that operate at over temperatures and pressures [9],[10]. As a result, combining dissimilar metals via welding is typically more difficult than joining identical metals. The microstructural changes and chemical gradients that result in notable variations in the structural, chemical, and physical properties of heterogeneous metal weldments.

II. THEORETICAL REFERENCE

The use of filler metal, which is frequently used in heterogeneous metal welding, adds even more complication [11]. The dissimilar metals that are commonly utilised for welded connections in the nuclear and chemical sectors were examined by [12], [13] examined the microstructural growth and corrosion behaviour of several 304/430 stainless steel welded joints. Sun et al. looked at the weldability and properties of austenitic or martensitic stainless-steel junctions. [14].

Gaurav Dak and Chandan Pandey conducted experimental investigation on the microstructure, mechanical characteristics,and stress residuals of a dissimilar welded junction composed of austenitic AISI 304L and martensic P92 stainless steel [15].When [16] Incoloy 800 and Inconel 600 Interlayer can somewhat minimize carbon migration.

In order to attain the desired qualities, welding must be done using optimal settings in every given procedure. Utilizingthe scientific method yields the ideal process parameters. The process parameters have been optimized in the current study using the Taguchi-based grey relational analysis approach. The application of optimization approaches for fusion and non-fusion welding, including the TIG welding process of dissimilar metals, has been demonstrated by several researchers. [17].

GRA was used to analyze the study's outcomes. Using the Taguchi Based GRA Method, Prabhakaran et al.'s study from [18] looked at how different laser welding parameters affected the hardness and tensile strength of different laser welding techniques. An optimization algorithm to maximize the Taguchi- based GRA's TIG welding capability for the Incoloy 8800HT.
[19] study from 20 centered on utilizing Taguchi-based GRA by [20]. The results of the study have been reported by all authors, demonstrating not only the effectiveness of optimization techniques for the optimization of TIG welding processes for different metals, but also demonstrating the scientific advantage of reducing the number of attempts to reach a desired weld property.

II.1 RESEARCH GAP

It has been observed in the literature that the mechanical and metallurgical characteristics of a joint are affected by welding parameters, including arc-gap measurement, weld bead measurement, torch speed measurement, welding current measurement, electrode apex measurement, welding voltage measurement, shielding gas measurement, etc. The quality and production of the industrial sectors will be significantly impacted by these welding parameters. For the manufacturer, controllingthe process input parameters has proven to be a challenging issue because, in order to achieve a suitable joint with the desired weld quality, parameters must be optimized before welding begins. When parameters are not optimized, distortion, flaws, and faults may be found.

In the current work, the Taguchi L9 orthogonal array in conjunction with GRA was used to improve the TIG welding procedure settings for the AISI 316-ASS to AISI 410-MSS connection. The tests were carried out by varying the shielding gas flow rate, welding speed, and current using a Taguchi L9 orthogonal array. For analytical purposes, the mean of the replies was determined. The best parameters were then determined by doing an ANOVA. The analysis yielded the ideal parameters, which were then empirically confirmed. The findings were then presented and debated. To investigate the tensile strength, microhardness, HAZ, its WZ, and chemical composition, transverse cuts were made in the welds.

III. MATERIALS AND METHODS

The base metals in this investigation were AISI 410-MSS and AISI 316-ASS. Table 1 provided a list of the basic metals' chemical compositions. Table 2 lists the basic metals' mechanical characteristics. The dimensions of the machined welding work parts were 100 mm × 70 mm × 3 mm. Each work component was butt joined using TIG welding after being cleaned with acetone. The base metals microstructure is depicted in figure 1.a and 1.b; AISI 410-MSS stainless steel has austenitic and twin crystal structures, whereas AISI 316-ASS stainless steel has martensite and ferrite structures. Different process settings (current 100, 120, and 140 amps; welding speed 1, 1.5, and 2 m/min; shielding gas flow rate 8, 10, and 12) were employed to alter the welds' mixing ratio.

Figure 1.a: ASS-316 base metals' microstructure.
Source: Authors, (2024).

Table 1: The weight percentages of the filler and base metals' chemical compositions.

Materials	AISI 316	AISI 410	ER316
C	0.024	0.15	0.04 -.08
Si	0.28	1.0	0.30-0.65
Mn	1.44	1.0	1.0-2.5
P	0.041	0.04	0.03
S	0.017	0.03	0.03
Cr	16.95	11.5-3.5	18-20
Mo	2.06	-	2-3

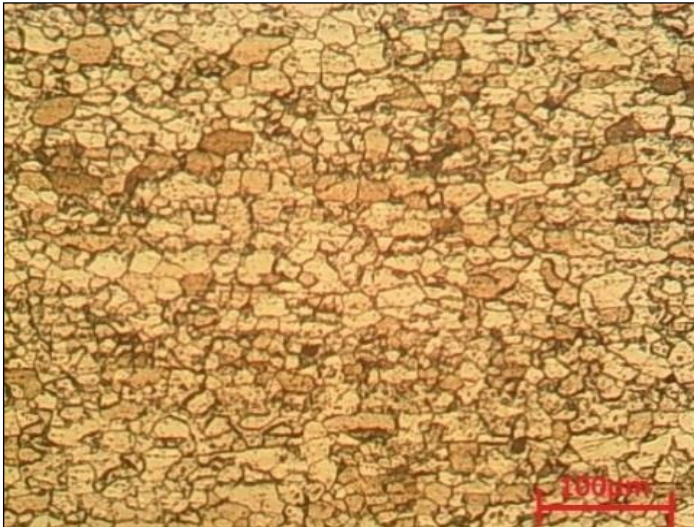| Materials	AISI 316	AISI 410	ER316
Ni	10.09	0.75	11-14
Fe	Balance	Balance	Balance

Source: Authors, (2024).

Figure 1.b: The MSS-410 basic metals' microstructure.
Source: Authors, (2024).

The shielding gas (lit/min) for each unique connection was argon. A range of significant process variables were determined through feasibility research. The maximum, middle, and lower levels of the TIG welding process parameters were found by a number of test runs; Table 2 shows these levels.

Table 2: Parameters of the TIG welding process and their values.

S.No		1	2	3
Process parameters		Current	Welding Speed	Shielding Gas Flow Rate
Units		amps	m/min	lit/min
Notation		A	S	G
Levels	**-1**	100	1	8
	0	120	1.5	10
	+1	140	2	12

Source: Authors, (2024).

The OA was chosen, and the tests were conducted in line with that choice. Micro hardness and Ultimate Tensile Strength (UTS) were selected as the goal functions. The ASTM E-08 standard was adhered to in the preparation of the tensile test specimen depicted in figure 2. Wire-cut EDM was used to cut test specimens for tensile strength. The TUE-CN-400 universal testing machine has been used to do tensile testing. The dissimilar welded joint's microstructure was made visible using aqua regia etchant. An etchant consisting of HCl: HNO3 = 3:1 was used. Using an OM Microscopy and SEM; Bruker outfitted with an EDS, the microstructures of the different welded samples were examined. EDS study was used to identify the weldment's chemical compositions.
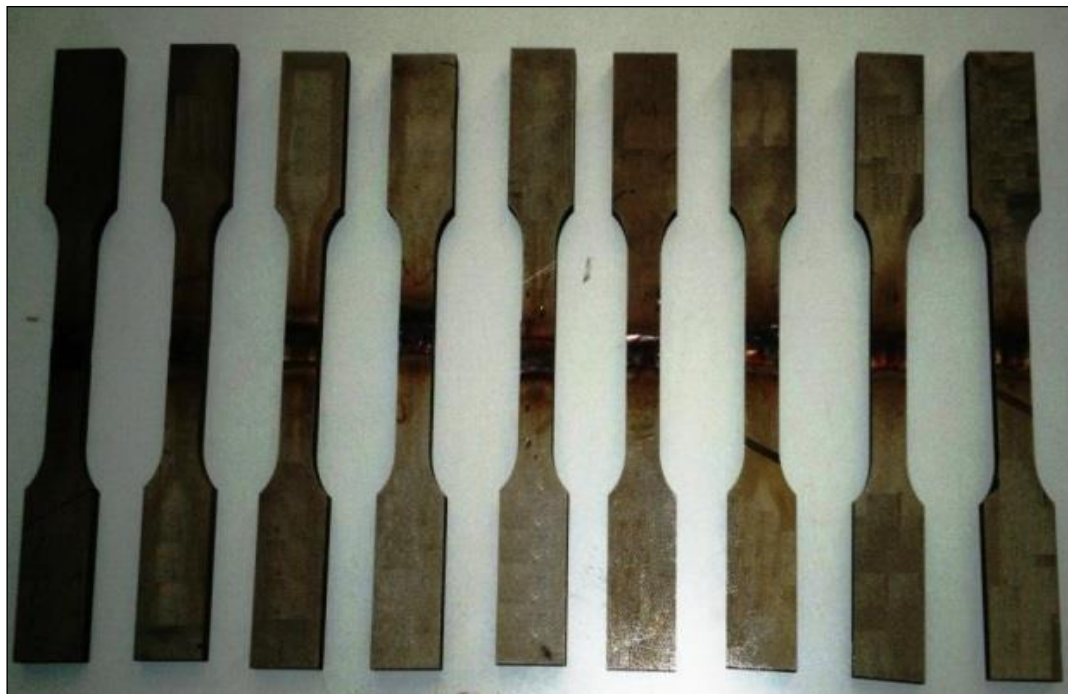

Figure 2: specimens tensile in accordance with ASTM E-08 standards.
Source: Authors, (2024).

IV. RESULTS AND DISCUSSION

Among the statistical performance metrics included in the Taguchi approach is the SNR. It is employed to gauge how well control elements that reduce product or process variation are detected. NB, LB, or HB are the three standard SNRs. SNR can be calculated independently for each quality characteristic and a high SNR indicates the best quality characteristics. The transition from the initial response values to the SNR is the pioneer step of the grey relationship analysis. Equation (1) of "Larger-the-Better"

was applied in this case. These SNR data served as the basis for further investigation. Table 3 displays the results for microhardness, computed SNR and (UTS) ultimate tensilestrength. Better strength performance is shown in the presentexperiment by higher ultimate tensile strength and microhardness

values. Therefore, for microhardness and tensile strength, the "higher-the-better" criterion was used.

$$S/N = -10\log_{10}[\sum(1/y)^2/n] \quad (1)$$

Table 3: Responses and SNR.

Run order	A amps	S m/min	G lit/min	UTS Mpa	HR HV1	SNR TS	SNR HR
1	100	1	8	483.617	197	53.69	45.89
2	100	1.5	10	492.298	198	53.84	45.93
3	100	2	12	495.152	201	53.89	46.06
4	120	1	10	491.593	207	53.83	46.32
5	120	1.5	12	497.512	199	53.94	45.98
6	120	2	8	494.356	200	53.88	46.02
7	140	1	12	486.984	202	53.75	46.11
8	140	1.5	8	493.467	206	53.87	46.28
9	140	2	10	491.873	221	53.84	46.89

Source: Authors, (2024).

$$x_i = (y_i(k) - \min y_i(k))/(\max y_i(k) - \min y_i(k)) \quad (2)$$

Equation (2) states that in GRG, the higher-the-better criterion is the outcome of the normalized tensile strength and microhardness. 4 presents the normalized investigational data in the range of 0-1 in GRA. The Grey Relational Coefficient (GRC) was assessed using this normalized data. Following the average of the GRC values associated with certain experimental outcomes, the Grey Relational Grade (GRG) was determined.

Equation (2) specifies the sequence after which the data are pre-processed and the corresponding comparability sequence is determined. (table 4) For WS, the corresponding sequence is k = 1; for experiments 1 to 9, the corresponding sequential sequence is k = 2. For microhardness, the correspondingsequences are i=1, 2=3=9. The remaining calculations were then

performed and all sequences after the pre-processing are consumed, as outlined in equation (3).

$$\Delta_{0i}(k) = |x_0(k) - x_i(k)| \quad (3)$$

Consequently, 0.5 and 0.5 are the weights that are used for microhardness and ultimate tensile strength, respectively. The grey relationship coefficient was computed using the weightage that was assigned. The GRG will be derived using table 5, which shows the GRC (ξ) that was calculated using equation (4), equation (5), as tabulated in table 6.

The variable n in this calculation denotes the total number of process answers.

Table 4: Grey relational generations of each performance characteristics and deviation sequences.

Run order	Sequences of Performance		Deviation Sequences	
	UTS Larger-the-better	HR Larger-the-better	UTS $\Delta_{0i}(1)$	HR $\Delta_{0i}(2)$
1	0.0000	0.0000	1.0000	1.0000
2	0.6248	0.0417	0.3752	0.9583
3	0.8302	0.1667	0.1698	0.8333
4	0.5740	0.4167	0.4260	0.5833
5	1.0000	0.0833	0.0000	0.9167
6	0.7729	0.1250	0.2271	0.8750
7	0.2423	0.2083	0.7577	0.7917
8	0.7089	0.3750	0.2911	0.6250
9	0.5942	1.0000	0.4058	0.0000

Source: Authors, (2024).

$$\xi_i(k) = \frac{\Delta_{min} + \psi\Delta_{max}}{\Delta_{0i}(k) + \psi\Delta_{max}} \quad (4)$$

$$\gamma_i = \frac{1}{n}\sum_{k=1}^{n}\xi_i(k) \quad (5)$$

Table 5: Relational coefficients in grey.

Run order	Grey Relational Coefficient	
	UTS $\xi_i(1)$	H $\xi_i(2)$
1	0.3333	0.3333
2	0.5713	0.3429
3	0.7465	0.3750
4	0.5400	0.4616

Run order	Grey Relational Coefficient	
	UTS ξ_i (1)	H ξ_i (2)
5	1.0000	0.3529
6	0.6877	0.3636
7	0.3976	0.3871
8	0.6320	0.4444
9	0.5520	1.0000

Source: Authors, (2024).

Table 6: Grey relational grades.

Run Order	GRG	Rank
	$\gamma_i = 1/2 \, (\xi_i \, (1) + \xi_i \, (2))$	
1	0.3333	9
2	0.4571	7
3	0.5608	3
4	0.5008	6
5	0.6765	2
6	0.5257	5
7	0.3924	8
8	0.5382	4
9	0.7760	1

Source: Authors, (2024).

Table 6 displays the GRG value to be used for the calculation of SNR; Table 7 displays SNR relation based on the higher the better the overall GRG criterion; and figure 3 displays the SNR curve which is a graphical representation to identify the optimal set of parameters. The SNR is a ratio between the signal and the noise, so if a high ratio is present, the desired result is achieved with very low noise. Figure 3 shows the current, welding speed, and shielding gas flow.

Table 7: SNR for GRG.

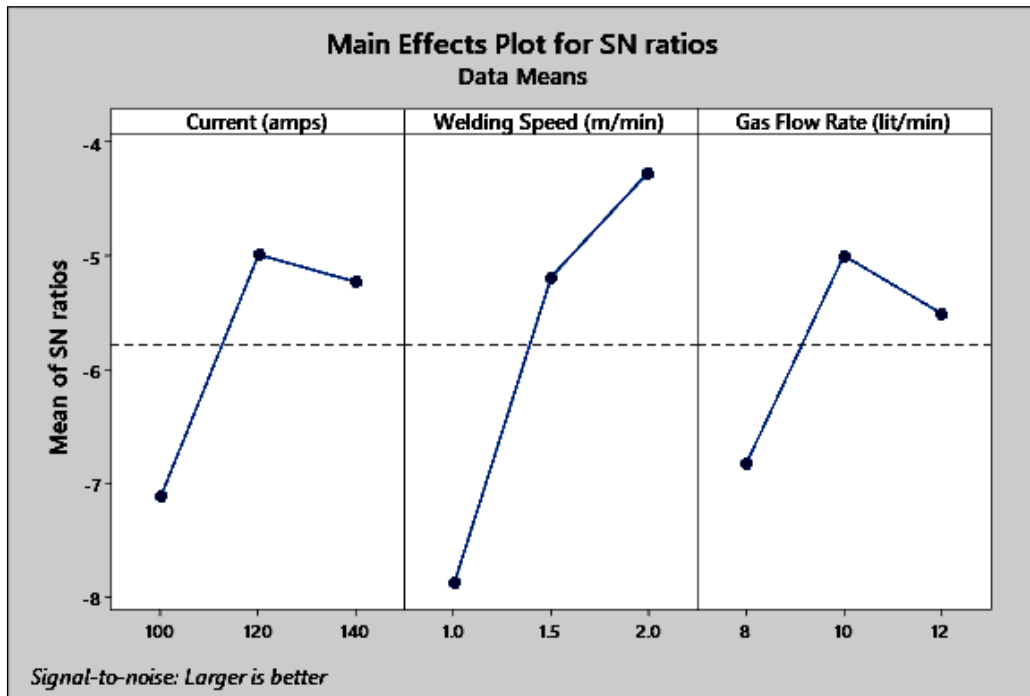| Run order	SNR for GRG
1	-9.54329
2	-6.79978
3	-5.02384
4	-6.00671
5	-3.39464
6	-5.58524
7	-8.12542
8	-5.38113
9	-2.20277

Source: Authors, (2024).

Figure 3: Main effects plot for SNR.
Source: Authors, (2024).

Table 8: Table of responses for GRG.

S. No	Process parameters	Levels			Range	Rank
		-1	0	+1		
1	A (amps)	0.4504	0.5676	0.5688	0.1368	2
2	S (m/min)	0.4088	0.5572	0.6208	0.2121	1
3	G (lit/min)	0.5952	0.4584	0.5332	0.1184	3

Source: Authors, (2024).

The welding speed has the most influence on responses, as can be observed from accordance table 8, where the weldingspeed range is maximum, this is consistent with data that other researchers have found previously [17 - 19] about various welding procedures and other materials. The research indicates that the ideal set of variables is 120 amps of current, 2 m/min of welding velocity, and 10 lit/min of shielding gas flow rate. Verification testing must be done using TIG welding and the ideal process

parameters found from the analysis since the optimal set of TIG welding process parameters determined by GRG is not in the L_9 orthogonal array implemented to conduct the trials.

IV.1 ANALYSIS OF VARIANCE

To determine which parameter has the greatest desired influence on the mechanical characteristics, an ANOVA was conducted. All of the process parameters are crucial since they all have substantial F values. (Table 9) Accordingly, the welding speed also had the biggest influence on the results in this examination, which is in line with the findings of earlier studies for a variety of other materials.

Table 9: ANOVA.

Source	DOF	Adj. SS	Adj. MS	F-Value	P-Value	Contribution
A (amps)	2	0.4744	0.2372	2.40	0.294	21.65
S (m/min)	2	1.2224	0.6112	6.19	0.139	55.78
G (lit/min)	2	0.2972	0.1485	1.51	0.399	13.56
Error	2	0.1974	0.0986			
Total	8	2.1914				

Source: Authors, (2024).

IV.2 MICROSTRUCTURAL STUDIES OF DISSIMILAR WELD ZONE

Investigations were conducted into the ideal heterogeneous welded joint of microstructure, alloying element distribution, and mechanical characteristics. The morphological characteristics of the dissimilar welded joints made using ER316 filler metal and AISI 410-MSS to AISI 316-ASS, respectively, are displayed in figure 4. To develop mirror-polished samples, dissimilar welded samples were cut from the cross-welds, ground, and polished. Aqua regia etchant was utilised to disclose the microstructure of the dissimilar welded junction. While the base metals of AISI 316-ASS stainless steel were composed of twin crystal and austenitic structures, those of AISI 410-MSS stainless steel were composed of martensite and ferrite structures.

Figure 4.a shows the optical architecture of the AISI 410-HAZ. Grain size in AISI 410-MSS increased progressively from the HAZ edge to the fusion boundary. As the distance from the weld contact decreased, the HAZ peak temperature actually rose, and grain development also depended on temperature. The HAZs of the two BMs were not the same. Figure 4.b illustrates the discovery of untreated ferrite δ stringers within the austeniticmatrix in the AISI 316 HAZ during the welding process, as documented in reference [21].

Ferrite can have an impact on the attributes of AISI 316, leading to low fatigue resistance and great corrosion resistance because of the high chromium concentration. Furthermore, the grains' expansion may be slowed by the ferrite. Moreover, the existence of δ ferrite may limit the formation of AISI 316-HAZ grains [22].

Figures 4.c and 5 show the architecture of the dissimilar weld zone (WZ), which is based on the content of the filler metal. The optical microscope observation in WZ showed a skeletalferrite microstructure inside a major austenitic matrix.
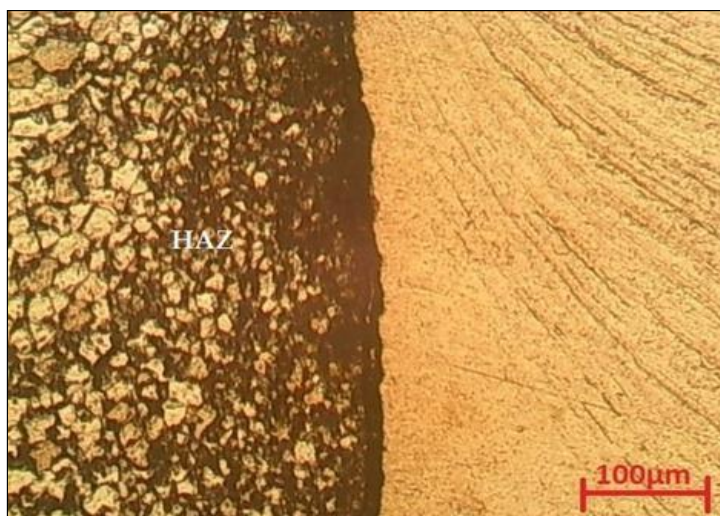

Figure 4.a: Microstructure of AISI 410-HAZ.
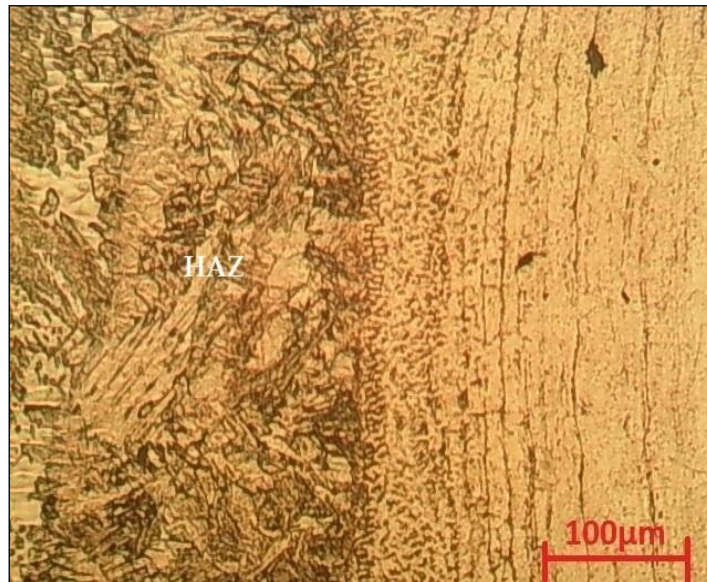Source: Authors, (2024).

Figure 4.b: Microstructure of AISI 316-HAZ.
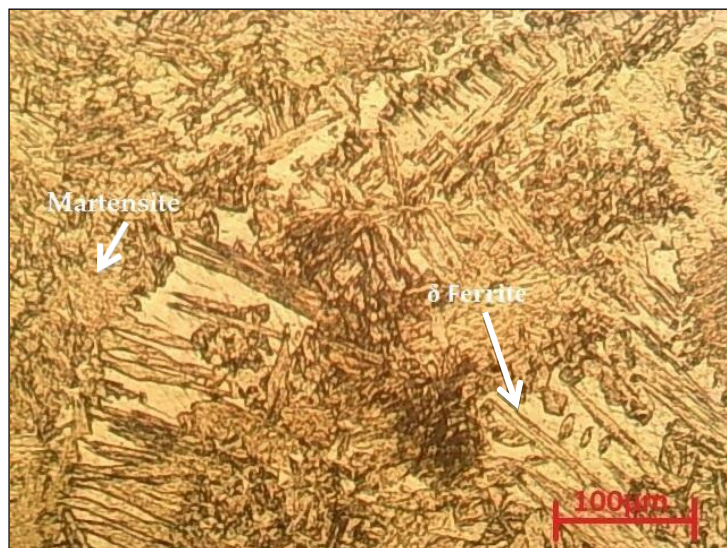Source: Authors, (2024).

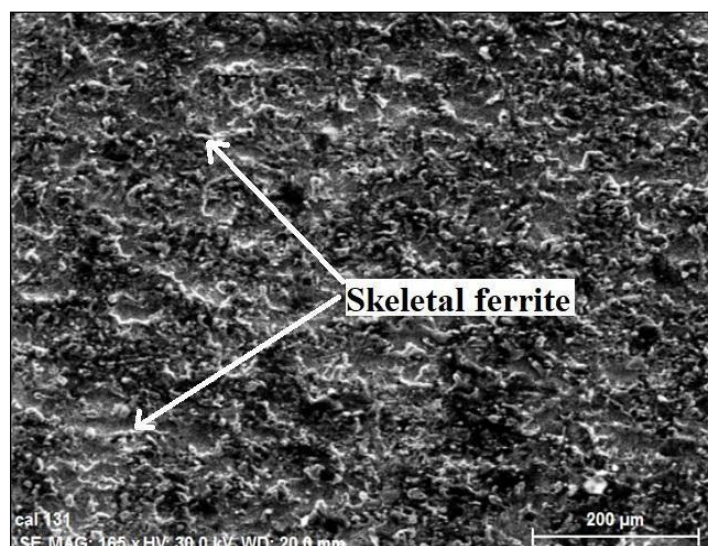Figure 4.c: Microstructure of Dissimilar weld zone.
Source: Authors, (2024).

Figure 5: SEM image of a different weld zone.
Source: Authors, (2024).

IV.3 DISTRIBUTION OF ALLOYING COMPONENTS IN WELD ZONE

The distribution of alloying elements in the dissimilar joint was investigated using the EDS mapping technique. The AISI 316/AISI 410 stainless steel filler metal's composition was different from the base materials in the dissimilar welding junction. This alternative filler material can avoid weldcracking and generate the necessary weld metal feature, but it also has the potential to impair the weld quality by causing macro-segregation at the fusion boundary. Bulk welding is created when molten base alloy comes into contact with droplets of the dissimilar filler material during the welding process. According to the line mapping study, no appreciable variations were seen at the weld zone. The elemental mapping investigation showed that Fe, Cr, Ni, Mn, Zn, and Cu were found in similar amounts to figure 6. Figure 7 shows the site where the EDS analysis showed that the fusion zone and the matrix contained nearly similar percentages of elements.
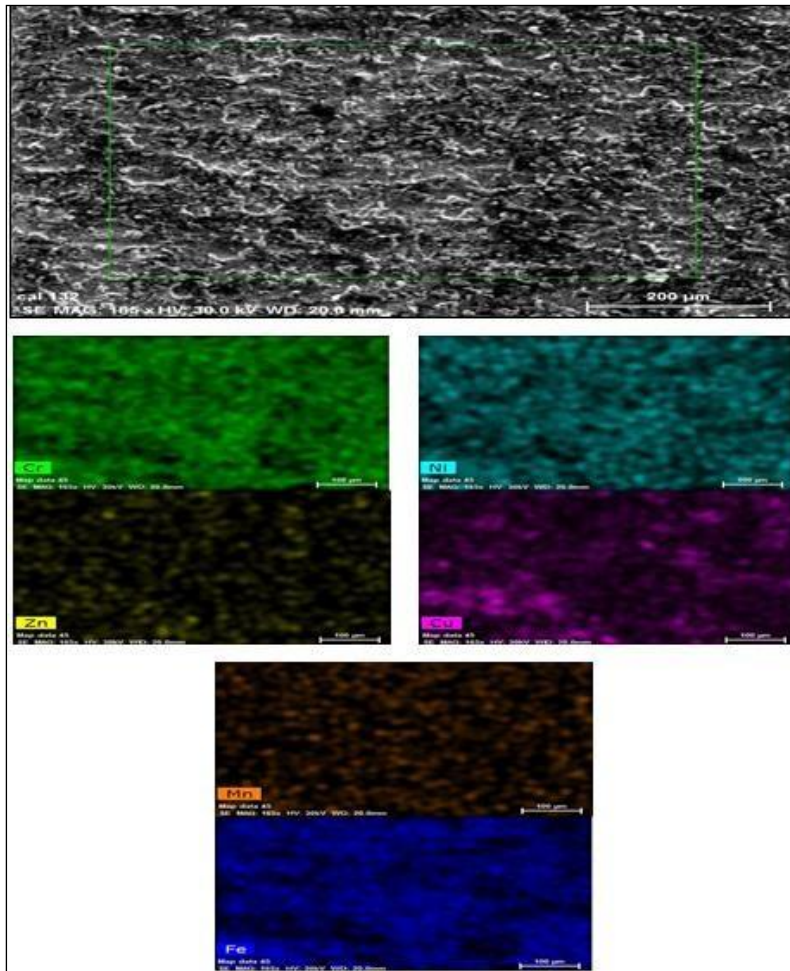

Figure 6: Distribution of alloying elements in Dissimilar weld zone.
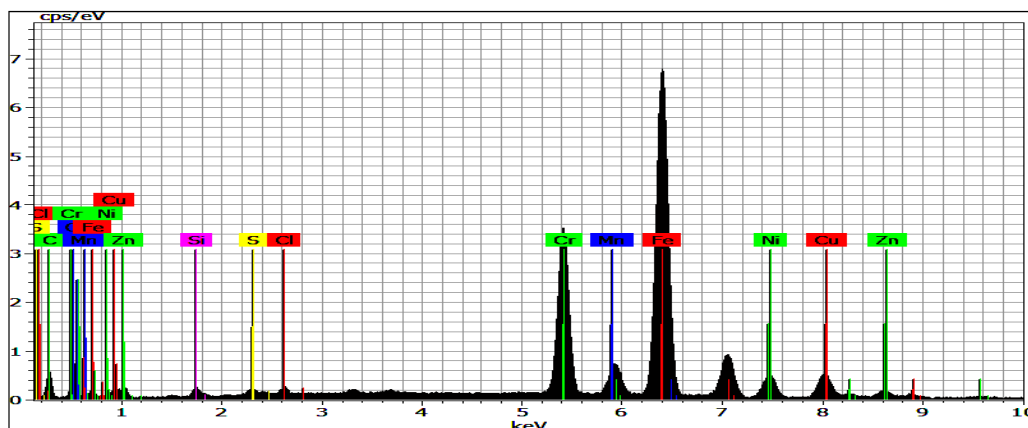Source: Authors, (2024).

Figure 7: EDS Point Analysis in the weld zone.
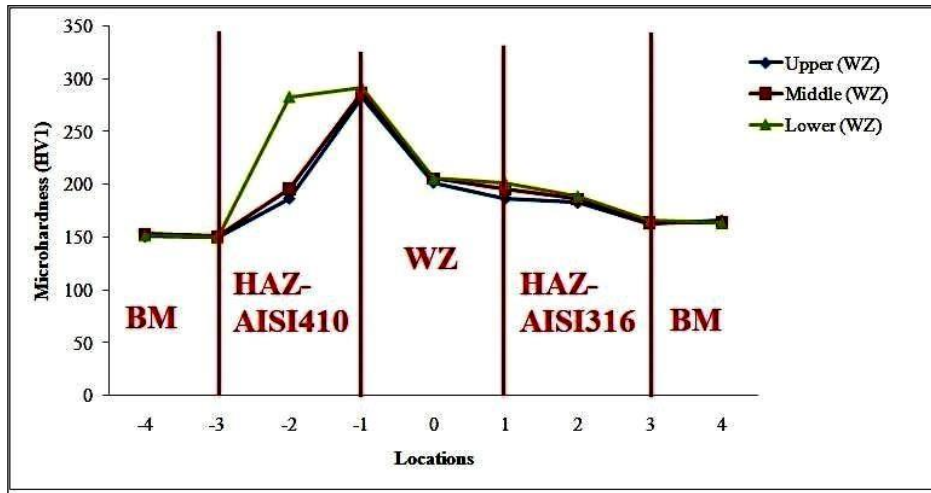Source: Authors, (2024).

Figure 8: Microhardness Profile.
Source: Authors, (2024).

IV.4 MECHANICAL PROPERTIES OF DISSIMILAR WELD JOINT

Welding was used to create an efficient and faultless dissimilar metal connection between AISI 316 and AISI 410. In the dissimilar weld zone, the mechanical characteristics of tensile and hardness were discovered. The martensite-Heat Affected Zone's tensile strength failure cannot deform as much or as soon as the base metal and weld due to the high martensite content. Thus, martensite formation and grain growth are the main factors influencing tensile strength in HAZ on the AISI 410 side.

The microhardness profile at the top, middle, and bottom of the weld's cross section is shown in Figure 8. The presence of the martensitic microstructure increased the hardness of the weld zone. Every joint exhibited the highest level of microhardness and the same pattern.

V. CONCLUSIONS

Based on the successful and flawless heterogeneous welding of 410-Martensite and 316-Austenitic stainless steel in this investigation, the following conclusions might be drawn:

- It was determined that the optimal combination of three GRG test parameters for quality weld joints is 120 amps for welding current; 2 m/min for welding speed; and 10 lit/min for shielding gas flow rate.
- The welding velocity contributed the most (55.78%) among the experimental parameters, followed by the shielding gas flow rate (13.56%) and current (21.65%), according to ANOVA.
- The different WZ's morphology showed an integrated structure made up entirely of fragile ferrite and a mostly austenitic matrix with no flaws. Heat affected zone in AISI 316 was typically composed of an austenite matrix with low δ ferrite content. The ferrite grain boundaries in the Martensite 410-heat affected zone included a continuous coating of martensite that had developed at a high temperature.
- In dissimilar weld joint, the alloying elements were uniformly distributed in the WZ confirmed through EDS mapping analysis.
- A rise in microhardness upto a median measurement of around 205 HV further demonstrated the predominant

austenitic matrix and skeletal ferrite nature of the WZ microstructure.

VI. AUTHOR'S CONTRIBUTION

Conceptualization: Kathiresan G, Vairavel M and Prabakaran M P.
Methodology: Kathiresan G and Prabakaran M P.
Investigation: Prabakaran M P and Govindarasan D
Discussion of results: Kathiresan G, Govindarasan D and Prabakaran M P.
Writing – Original Draft: Kathiresan G.
Writing – Review and Editing: Prabakaran M P.
Resources: Govindarasan D.
Supervision: Dr. Vairavel.M
Approval of the final text: Kathiresan G, Vairavel.M and Prabakaran M P

VII. REFERENCES

[1] J. CaoJ, Y. Gong, Z. Yang, X. Luo, F. Gu and Z. Hu, "Creep fracture behavior of dissimilar weld joints between T92 martensitic and HR3C austenitic steels", International Journal of Pressure Vessels and Piping, vol. 88, no. 2-3, pp. 94-98, Feb – Mar.2011.

[2] B. Shanmugarajan, P. Sathiya and G. Buvanashekaran, "Mechanical and metallurgical properties of autogenous laser welded P92 material", Journal of Manufacturing Process, vol. 24, pp. 11– 18, Oct.2016.

[3] J. Ni, X. Wang, J. Gong and M. Abdel, "Thermal, metallurgical and mechanical analysis of circumferentially multi-pass welded P92 steel pipes", International Journal of Pressure Vessels and Piping, vol. 165, pp. 164–175, Aug. 2018.

[4] G. Dak, J. Joshi, A. Yadav, A. Chakraborty, N. Khanna, "Autogenous welding of copper pipe using orbital TIG welding technique for application as high vacuum boundary parts of nuclear fusion devices", International Journal of Pressure Vessels and Piping, vol. 188, no. 104225, Dec. 2020.

[5] C.R. Das, A.K. Bhaduri, G. Srinivasan, V. Shankar and S. Mathew, "Selection of filler wire for and effect of auto tempering on the mechanical properties of dissimilar metal joint between 403 and 304L(N) stainless steels", Journal of Material Processing Technology, vol. 209, no. 3, pp. 1428-1435, Feb. 2009.

[6] A.N. Isfahany, H. Saghafian and G. Borhani, "The effect of heat treatment on mechanical properties and corrosion behavior of AISI 420 martensitic stainless steel", Journal of Alloys Compounds, vol. 509, no. 9, pp. 3931-3936, Mar. 2011.

[7] P. Cisquini, S.V. Ramos, P.R.P Viana, V.F. Cunha Lins, A.R. Franco Jr and E.A. Vieira, "Effect of roughness produced by plasma nitro carburizing on

corrosion resistance of AISI 304 austenitic stainless steel", Journal of Materials Research and Technology, vol. 8, no. 2, pp. 1897-1906, Feb. 2019.

[8] R. Kacar and O. Baylan, "An investigation of microstructure/property relationships in dissimilar welds between martensitic and austenitic stainless steels", Materials & Design, vol. 25, no. 4, pp. 317-329, Jun. 2004.

[9] J. Bin Wen, C.Y. Zhou, X. Li, X. M. Pan, L. Chang, G.D. Zhang et al, "Effect of temperature range on thermal-mechanical fatigue properties of P92 steel and fatigue life prediction with a new cyclic softening model", International Journal of Fatigue, vol. 129, no. 1, Aug. 2019.

[10] W.G. Seo, J.Y. Suh, J.H. Shim, H. Lee, K. Yoo, S.H. Choi SH, "Effect of post-weld heat treatment on the microstructure and hardness of P92 steel in IN740H/P92 dissimilar weld joints", Material Characterization, vol. 160, no. 110083, Feb. 2020.

[11] M.P. Prabakaran, G.R. Kannan, "Effect of post weld heat treatment on dissimilar laser welded joints of austenitic stainless steel to low carbon steel", International Journal of Pressure Vessels and Piping, vol. 191, no. 104322, Jun. 2021.

[12] Abishek Ghosh and Pradip Kumar Pal, "Corrosion behaviour of dissimilar TIG welded austenitic stainless steel AISI 304 and martensitic stainless steel AISI 420", Indian Journal of Engineering & Materials Sciences, vol. 27, no.3, pp. 665- 669, Jun. 2020.

[13] Caimei Wang, Yang Yu, Jianxing Yu, Zhang Yu, Yan Zhao, Qiwei Yuan, "Microstructure evolution and corrosion behavior of dissimilar 304/430 stainless steel welded joints", Journal of Manufacturing Processes, vol. 50, pp. 183–191, Feb. 2020.

[14] Z. Sun and H.Y. Han, "Weldability and properties of martensitic/ austenitic stainless steel joints", Materials Science and Technology, 1994; vol. 10, no. 9, pp. 823-829, Jul. 1994.

[15] Gaurav Dak and Chandan Pandey, "Experimental investigation on microstructure, mechanical properties, and residual stresses of dissimilar welded joint of martensitic P92 and AISI 304L austenitic stainless steel", International Journal of Pressure Vessels and Piping, vol. 194, no. 104536, Dec. 2021.

[16] A. Kulkarni, D.K. Dwivedi, M. Vasudevan, "Dissimilar metal welding of P91 steel- AISI 316L SS with Incoloy 800 and Inconel 600 interlayers by usingactivated TIG welding process and its effect on the microstructure and mechanical properties", Journal of Material Processing Technology, vol. 274, no. 116280, Dec. 2019.

[17] N.P. Chandresh, S. Chaudhary, "Parametric optimization of weld strength of metal inert gas welding and tungsten inert gas welding by using analysis of variance and grey relational analysis", International Journal of Research in Modern Engineering and Emerging Technology, vol. 1, no. 3, pp. 48–56, Apr. 2013.

[18] M.P. Prabakaran and G.R. Kannan, "Optimization of laser welding process parameters in dissimilar joint of stainless steel AISI316 / AISI1018 low carbon steel to attain the maximum level of mechanical properties through PWHT", Optics and Laser Technology, vol. 112. pp. 314–322, Apr. 2019.

[19] B. Shanmugarajan, Rishabh Shrivastava, P. Sathiya, G. Buvanashekaran G, "Optimization of laser welding parameters for welding of P92 material using Taguchi based grey relational analysis", Defence Technology, vol. 12, pp. 343– 350, Aug. 2016.

[20] Arun Kumar Srirangan, Sathiya Paulraj, "Multi-response optimization of process parameters for TIG welding of Incoloy 800HT by Taguchi grey relational analysis", Engineering Science and Technology: An International Journal, vol. 19, pp. 811–817, Jun. 2016.

[21] Giuseppe Casalino, Andrea Angelastro, Patrizia Perulli, Caterina Casavola, Vincenzo Moramarco, "Study on the fiber laser/TIG weldability of AISI 304 and AISI 410 dissimilar weld", Journal of Manufacturing Processes, 2018; vol. 35, pp. 216-225, Oct. 2018.

[22] G.Casalino and F. Panella. "Microstructural analysis of AISI 304 bars welded with high speed pulsed discharges", Journal of Material Processing Technology, vol. 191, pp. 149–152, Aug. 2007.